J. Fluid Mech. (1994), vol. 272, pp. 183–209

Turbulence structural changes for a three-dimensional turbulent boundary layer in a 30° bend

By WALTER R. SCHWARZ† AND PETER BRADSHAW
Department of Mechanical Engineering, Stanford University, Stanford, CA 94305, USA

(Received 29 January 1993 and in revised form 28 February 1994)

A three-dimensional turbulent boundary layer (3DTBL) was generated on the floor of a low-speed wind tunnel by the imposition of a cross-stream pressure gradient using a 30° bend in the horizontal plane. The surface streamlines were deflected by as much as 22° relative to the local tunnel centreline. Downstream of the bend, the 3DTBL gradually relaxed towards a 2DTBL; this was an impulse-and-recovery experiment which focused on the outer layer. Mean velocities were measured with a three-hole yawmeter and turbulence quantities, which included the Reynolds-stress tensor and the triple products, were measured with a cross-wire hot-wire anemometer. The experiment isolated the effects of crossflow from those of adverse streamwise pressure gradients, which may have clouded interpretations of previous 3DTBL experiments. In particular, the detailed developments of the cross-stream shear stress and of the stress/energy ratio become clearer. The shear-stress vector lagged behind the velocity-gradient vector as crossflow developed; however, the two vectors became more closely aligned downstream of the bend. Reductions in the stress/energy ratio implied that crossflow made shear-stress production less efficient. Another effect of three-dimensionality was a change of sign in the vertical transport of turbulent kinetic energy by turbulence, in the inner part of the boundary layer.

1. Introduction

Many flows such as those over swept wings of aircraft and also those inside turbomachines are strongly influenced by three-dimensional turbulent boundary layers (3DTBLs). Currently, full time-dependent Navier–Stokes solutions for turbulent flow simulations are too expensive for engineering use, so models are needed – usually based on time-averaged equations and needing empirical input in the forms of structural coefficients of the turbulence. Frequently, when turbulence models developed for 2DTBLs are extended to 3DTBLs, they give poor results owing to significant changes in turbulence structure. The performance of turbulence models applied to 3DTBLs was probably first systematically evaluated as part of the 'Trondheim Trials' reported by Fanneløp & Krogstad (1975). Since that time, several reviews including Johnston (1976), Lakshminarayana (1986), Launder (1988), van den Berg (1990), Bradshaw (1990), and Purtell (1992) have continued to recognize the need for more detailed turbulence measurements to help advance methods of modelling turbulence in 3DTBLs.

† Present address: Department of Mechanical Engineering, Stevens Institute of Technology, Hoboken, NJ 07030, USA

By definition, a 3DTBL has velocity gradients in the direction normal to the surface, the y-direction, which are large compared to those in the x- and z-directions (which are approximately the streamwise and spanwise directions respectively). In particular, the x-component vorticity is closely equal to $\partial W/\partial y$, $\partial V/\partial z$ being small. Also, $\partial W/\partial y$ contributes to the production term for the (y,z)-plane shear stress $-\overline{vw}$ which appears in the streamwise mean vorticity equation

$$U\frac{\partial \Omega_x}{\partial x} + V\frac{\partial \Omega_x}{\partial y} + W\frac{\partial \Omega_x}{\partial z} = \Omega_x\frac{\partial U}{\partial x} + \Omega_y\frac{\partial U}{\partial y} + \Omega_z\frac{\partial U}{\partial z} + \left(\frac{\partial^2}{\partial y^2} - \frac{\partial^2}{\partial z^2}\right)(-\overline{vw}) + \frac{\partial^2}{\partial y \partial z}(\overline{v^2} - \overline{w^2}) + \nu\nabla^2\Omega_x. \quad (1)$$

In a 3DTBL, mean streamwise vorticity is usually generated by skewing, resulting from (i) shearing forces applied to the fluid by a moving surface or (ii) the application of a cross-stream pressure gradient, which deflects the streamlines of the flow close to the surface more strongly than near the free stream. Thus, 3DTBLs are generally referred to as being either shear-driven or pressure-driven. Reynolds-stress gradients generally act to reduce skew-induced crossflow: we do not consider stress-induced crossflow, which is usually associated with large z-gradients.

3DTBL experiments have been reviewed by Johnston (1976), Fernholz & Vagt (1981), and Anderson & Eaton (1987). In 1976, Johnston cited over 80 experiments dealing with 3DTBLs. Only those experiments measuring all six components of the Reynolds-stress tensor can be used to help develop 3DTBL turbulence models. All too often, the shear stress $-\overline{vw}$ has been omitted because it is difficult to measure with either hot wires or laser-Doppler velocimeters. Using cross-wire hot-wire anemometers, the measurement is difficult because one cannot arrange the orientation of the wires in such a way as to be sensitive to only v- and w-fluctuations. Thus, one must combine measurements from two probe orientations sensitive to u and either $(v + w)/\sqrt{2}$ or $(v - w)/\sqrt{2}$ to get $-\overline{vw}$.

Most 3DTBL experiments have imposed a cross-stream pressure gradient on an initial 2DTBL. The experiments of Bradshaw & Terrell (1969), Johnston (1970), Elsenaar & Boelsma (1974), East & Sawyer (1979), and Bradshaw & Pontikos (1985) had spanwise-component flows that approximated untapered swept wings of infinite span ('infinite yawed flows'). 3DTBLs on the plane walls of curved rectangular ducts were studied by Pierce & Duerson (1975) and DeGrande & Hirsch (1978). Experiments on flows approaching obstacles include those of Pierce & Ezekewe (1976), Dechow & Felsch (1977), Müller (1982), and Anderson & Eaton (1989). Fernholz & Vagt (1981) studied the 3DTBL in inclined flow along a circular cylinder, approaching separation.

More recently, Flack & Johnston (1993) have performed water-channel experiments for a swept forward-facing step and also a 30° bend similar to that used here. The Flack & Johnston experiments concentrated on the inner layer, using laser-Doppler anemometry techniques. This was a deliberate splitting of the work: in our experiment, emphasis was on the outer-layer structure.

Shear-driven 3DTBL experiments, which typically involve flow along a rotating cylinder, include those of Bissonnette & Mellor (1974), Lohmann (1976), Driver & Hebbar (1987), and Driver & Johnston (1990). Another approach, implemented by Littell & Eaton (1991), was to generate a 3DTBL on a spinning disk. The shear drove the circumferential motion and the circumferential motion provided the 'centrifugal force' to drive the crossflow in the radial direction.

Direct numerical simulation of the full time-dependent Navier–Stokes solutions is now being widely used to obtain the same types of information as provided by traditional experiments and supply data for quantities that are difficult or impossible to measure. Recent direct simulations of 3DTBLs were performed by Spalart (1989), Coleman, Ferziger & Spalart (1990), Moin *et al.* (1990), and Sendstad & Moin (1991). Although direct numerical simulation has the potential for providing a wealth of valuable information on the inner layer, one must realize that it has so far been limited to $Re_\theta \leqslant 1500$ ($Re_\theta \equiv U_e\theta/\nu$) and therefore may not be wholly representative of the outer layer in boundary layers having high Reynolds numbers.

The simplest turbulence models for 3DTBLs define an eddy viscosity ν_T in terms of the mean-velocity gradients and the existing Reynolds stresses,

$$-\overline{uv} = \nu_T \frac{\partial U}{\partial y} \qquad \text{and} \qquad -\overline{vw} = \nu_T \frac{\partial W}{\partial y}. \tag{2}$$

A drawback to this approach is that the same 'isotropic' ν_T is used for both shear stresses despite data indicating that $-\overline{uv}$ and $-\overline{vw}$ may react differently to mean-velocity gradients; that is ν_T, as defined by (2), may be a vector. However, the x- and z-directions are arbitrary and it is not legitimate to make ν_T an explicit function of direction in the (x,z)-plane. More sophisticated turbulence models abandon the eddy-viscosity concept, and are based on the Reynolds-stress transport equations where advection, generation, pressure–strain redistribution, turbulent transport, viscous diffusion, and viscous destruction processes are accounted for.

If isotropic modelling were appropriate for 3DTBLs, the Reynolds stress $-\overline{vw}$ would grow immediately in response to crossflow as predicted by $-\overline{vw} = \nu_T \partial W/\partial y$. However, in many experiments, the response of $-\overline{vw}$ lags behind that predicted by isotropic eddy-viscosity models. The lag can be described using shear-stress and velocity-gradient vectors

$$\gamma_\tau \equiv \tan^{-1}\left[\frac{\overline{vw}}{\overline{uv}}\right] \qquad \text{and} \qquad \gamma_g \equiv \tan^{-1}\left[\frac{(\partial W/\partial y)}{(\partial U/\partial y)}\right]. \tag{3}$$

Isotropic eddy viscosity would imply $\gamma_\tau = \gamma_g$, but it is found that γ_τ usually lags behind γ_g as the latter increases with x, as is qualitatively shown by the exact transport equation for $-\overline{vw}$, whose generation term is $\overline{v^2}\partial W/\partial y$. Opposite trends ($\gamma_\tau$ leading γ_g) were seen by Lohmann (1976), Pierce & Ezekewe (1976), Fernholz & Vagt (1981), Müller (1982), and Driver & Hebbar (1987).

Departures from isotropic eddy viscosity can be shown using the eddy-viscosity ratio

$$N_e \equiv \frac{\nu_{T_{yz}}}{\nu_{T_{xy}}} = \frac{-\overline{vw}/(\partial W/\partial y)}{-\overline{uv}/(\partial U/\partial y)}, \tag{4}$$

which is arbitrarily defined depending on the coordinate system used. The eddy-viscosity ratio can also be written as

$$N_e = \frac{\tan(\gamma_\tau - \gamma_u)}{\tan(\gamma_g - \gamma_u)}, \tag{5}$$

where γ_u represents the direction of the local mean velocity, γ_g represents the direction of the mean-velocity gradient vector, and γ_τ represents the direction of the shear-stress vector. $N_e=1$ corresponds to isotropic eddy viscosity, and $N_e<1$ implies $|\gamma_\tau|<|\gamma_g|$.

Another frequently observed characteristic is that the ratio of turbulent shear stress

magnitude to twice the turbulent kinetic energy ($k \equiv \overline{q^2}/2 \equiv (\overline{u^2} + \overline{v^2} + \overline{w^2})/2$),

$$a_1 \equiv [(\overline{uv})^2 + (\overline{vw})^2]^{1/2} / \overline{q^2}, \tag{6}$$

decreases in the presence of crossflow. The a_1 parameter (independent of axes) can be crudely regarded as the efficiency of the eddies in producing turbulent shear stresses for a given amount of turbulent kinetic energy. Some investigators have found that decreases in a_1 were simply due to decreases in $-\overline{uv}$ when crossflow was applied to a 2DTBL, rather than to increases in $\overline{q^2}$. However, this was not always the case. In the experiments of Pierce & Duerson (1975), DeGrande & Hirsch (1978), Lohmann (1976), Anderson & Eaton (1989), Flack & Johnston (1993), and in the present work, the decrease in a_1 was accompanied by increases in turbulent shear stress in the outer layer. Whether the Reynolds stresses increase or decrease depends on the details of the flow, but it is clear that crossflow leads to less efficient production of turbulent shear stress.

Two theories for the reduction of a_1 have been put forth in the past few years. Bradshaw & Pontikos (1985) suggested that the observed reduction in a_1 was attributable to the sideways toppling of large eddies in the presence of a crossflow. The tilting of the large stress-producing eddies in the outer layer results in an orientation in which the production of shear stress by the large eddies is less efficient than it would be in a 2DTBL. Eaton (1991), expanding upon earlier work by Anderson & Eaton (1989), explained the reduction in a_1 as the result of changes in the flow structure near the wall. This was hypothesized to be due to the crossflow decreasing the number of low-speed streaks and stress-producing burst-sweep mechanisms. This explanation may not be relevant to the outer layer.

The objective of the present experiment is to study and explain the changes in turbulence structure that develop due to crossflow in the boundary layer, specifically in the outer layer where these changes appear to be largest. We have not attempted to probe the inner layer in detail: this is better done in a low-Reynolds-number experiment (see Flack & Johnston 1993). The work included mapping the mean flow field (velocity magnitude and direction), performing detailed turbulence measurements, determining the surface static pressure distribution, measuring the surface shear stress, and performing surface flow visualization. We decided to impose crossflow as suddenly as possible on a 2DTBL, because structural changes seem to be larger than in flows which have come more nearly into three-dimensional equilibrium (for example the Ekman layer of Coleman *et al.* 1990). The present experiment was also designed to provide new data that can be used in developing and testing turbulence models for 3DTBLs. An advance over previous work is that the measurements are detailed enough for all terms in all the Reynolds-stress transport equations to be evaluated, either directly or by difference, with some assumptions about unmeasurable terms.

2. Equipment and techniques

The experiment was conducted in an open-circuit blower tunnel, with a 762 mm × 762 mm test section and a maximum velocity of about 30 m s^{-1}. The longitudinal-component turbulence level in the working section was about 0.3%. The tunnel and techniques are described in more detail by Schwarz & Bradshaw (1992).

Figure 1 is a plan view of the test section and the 36 measurement locations. The measurements did not cover the full width of the test section, but as the upstream flow is two-dimensional the boundary conditions for a computation are adequately defined. A 3DTBL on the floor was generated by the imposition of a cross-stream

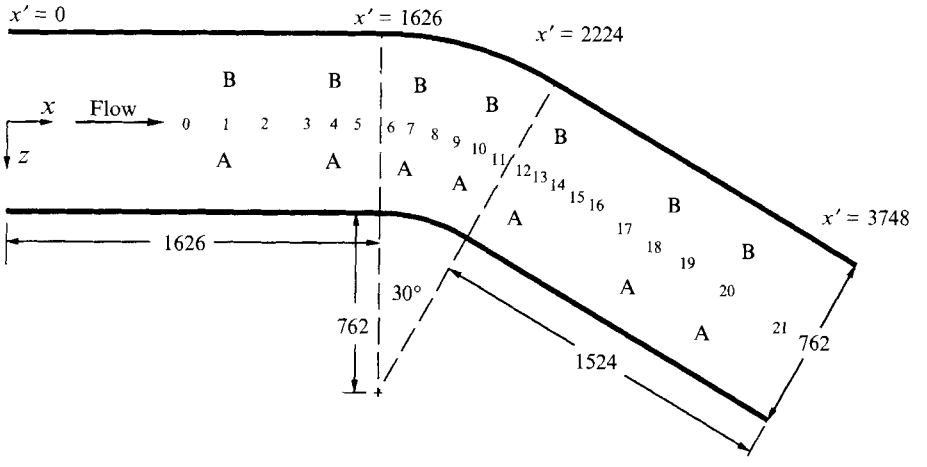

FIGURE 1. 3-hole yawmeter and hot-wire anemometer measurement locations (measurements in mm).

pressure gradient using a 30° bend in the horizontal plane. The bend geometry was used to provide a rapid increase of crossflow shear $\partial W/\partial y$ while maintaining a relatively small pressure gradient along the centreline of the test section. Downstream of the bend, the 3DTBL gradually relaxed towards a two-dimensional flow as the cross-stream pressure gradient diminished. To a first approximation, the flow was an initial 2DTBL perturbed by a nearly frozen $\partial W/\partial y$ field, created by the 30° bend, which permitted the study of response and recovery. Overall, there was a slight favorable streamwise pressure gradient due to boundary-layer growth.

The boundary layer on the floor of the working section was forced to become turbulent by a trip wire (1.6 mm diameter) placed at x'=0 mm, close to the contraction exit. At the first measurement station, x'=826 mm, the boundary layer was two-dimensional and had the following parameters: $\delta_{99} = 20.9$ mm, $\theta = \theta_{11} = 2.4$ mm, $H = H_{11} = 1.38$, $c_f = 0.0030$, and $Re_\theta = 4100$ at a free-stream velocity of $U_{\text{ref}} = 26.5$ m s^{-1}.

Surface flow visualizations with an oil mixture were used to estimate the surface streamline deflection. The mixture combined titanium dioxide powder, kerosene, and oleic acid (used as a dispersant) in the ratio 5:15:1 by volume.

The mean velocity field was measured using a three-hole yawmeter constructed from three hypodermic tubes (1.4 mm OD) with the end tubes chamfered at 35° angles as recommended by Bryer & Pankhurst (1971). A computer-controlled near-nulling method was used, which aligned the probe to within 1° of the flow direction. Final resolution of the flow direction was obtained using the probe yaw calibration performed in the free stream. This is much faster than accurate nulling. Wall proximity effects were accounted for by the Young & Maas (1936) correction. The uncertainty in velocity magnitude is estimated as ± 0.2 ms^{-1} and the flow direction uncertainty as $\pm 1°$.

Surface shear stresses were indirectly measured using the centre tube of the three-hole yawmeter as a Preston tube, with Patel's (1965) calibration. Although Patel's calibration was developed for a 2DTBL, it was assumed that in 3DTBLs having mild pressure gradients the law of the wall was valid for a distance up to the diameter of the Preston tube. This is consistent with the findings of Pierce, McAllister & Tennant (1983) and Degani, Smith & Walker (1992) on the existence of near-wall

similarity in pressure-driven 3DTBLs: see also Ölçmen & Simpson (1992) and Flack & Johnston (1993). The measurements were taken with the probe aligned with the mean flow near the wall.

Turbulence statistics, which included the six components of the Reynolds-stress tensor, the ten triple products, and the three fourth powers, were obtained using a home-built Microscale Systems HWM-100 constant-temperature anemometer with a Dantec model 55P51 cross-wire probe. The probe had two platinum-plated tungsten wires with 5 μm diameter and 1.25 mm active length, spaced 1 mm apart and set at angles of approximately $\pm 45°$ to the flow. Turbulence measurements were taken with the plane of the wires placed at four different roll angles: two were the (U,V) and (U,W) planes; the other two were at $\pm 45°$ to the (U,V) plane. When placed in the last two planes, the probe was sensitive to $(v+w)/\sqrt{2}$ or $(v-w)/\sqrt{2}$. Mean products involving both v- and w-fluctuations were determined by combining the statistics from the two 45° planes and thus were subject to some additional scatter.

The Bearman (1971) temperature correction was used to account for ambient temperature drift. The actual temperature variations during a typical two-hour run were less than 3K. The uncertainty due to flow normal to the plane of the wires and to prong interference was reduced by aligning the probe with the direction of the local mean velocity. Anderson & Eaton (1989) also used Dantec 55P51 cross-wire probes. Their estimated uncertainty values were 5% for $\overline{u^2}$, $\overline{v^2}$, and $\overline{w^2}$; 10% for $\overline{uv}$ and $\overline{uw}$; and 15% for $\overline{vw}$. Measurements in the 2DTBL region of the present experiment when compared to the Reynolds-stress measurements of Klebanoff (1954) agreed within these uncertainties. The 2DTBL measurements of the present experiment also agreed to within 20% of the peak values for the triple products measured by Murlis, Tsai & Bradshaw (1982).

The test section was traversed using a system which slid along rails mounted on the top of the test section. Stepper motors, controlled by a microcomputer, were used for vertical, spanwise, yaw, and roll movements of the probe.

3. Results and discussion

The results are presented with respect to one of two specified coordinate systems, depending on the subject being discussed. A fixed coordinate system aligned with the *upstream* test section is used to more clearly show departures from the initial 2DTBL. In this (x, y, z) coordinate system, the x-direction was along the centreline of the upstream test section, the y-direction was normal to the floor, and the z-direction was in the spanwise direction. The other coordinate system (x', y', z') was aligned with the *local* tunnel centreline. This coordinate system is used to show the axial development in general, and also to present the terms in the Reynolds-stress transport equations. In this system, the x'-direction was curvilinear as it followed the centreline of the tunnel, the y'-direction was again normal to the floor, and the z'-direction was in the local spanwise direction perpendicular to the x'-direction. The origins of x and x' were at the trip wire. For simplicity in notation, we use U, V, and W as the mean velocity components and u, v, and w as the fluctuating velocity components in both coordinate systems. All of the coordinate-dependent figures are labelled with their respective coordinate system.

The static pressure coefficient distribution, $c_p \equiv (p - p_{ref})/\frac{1}{2}\rho U_{ref}^2$, in figure 2 shows that c_p, defined with respect to reference static pressure at $x' = 0$ mm, ranged from −0.6 along the convex wall to 0.3 along the concave wall. The maximum dimensionless spanwise pressure gradient based on the local boundary-layer thickness (δ_{99}) and the

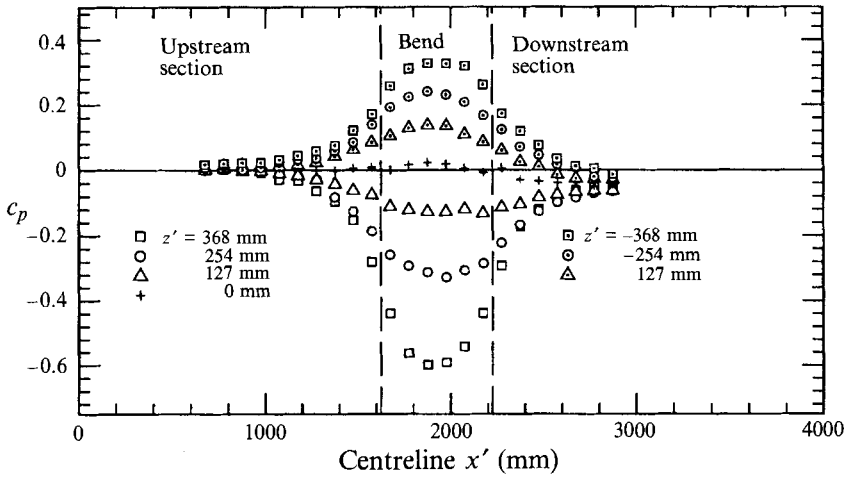

FIGURE 2. Static pressure coefficient distribution.

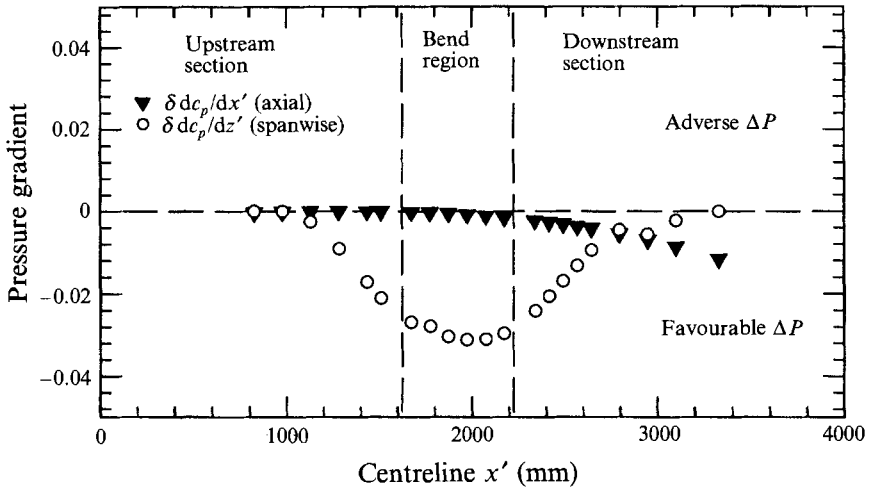

FIGURE 3. Axial and spanwise pressure gradients.

(x', y', z') coordinate system based on the local tunnel centreline, $\delta_{99}\partial c_p/\partial z'$, was −0.034 halfway through the bend. The axial pressure gradient, shown in figure 3, was nearly zero along the centreline until a slight favourable pressure gradient developed due to the thickening of the boundary layers downstream.

The oil-flow streamlines are shown in figure 4. The fine white streaks show that the surface flow direction was rapidly deflected at the beginning of the bend, and continued to turn through the bend until a maximum deflection of approximately 22° relative to the local tunnel centreline was reached. Downstream of the bend, the crossflow slowly decayed. Note that the streamlines starting from the outer wall did not reach the centreline until $x' \approx 2500$ mm. Along the centreline, downstream of $x' \approx 2500$ mm, only the viscous-sublayer and buffer-layer regions would have had fluid that started along the outer wall; however, the relatively small lengthscales of the flow in the sublayer and buffer layer make it unlikely that those profiles were significantly affected by the details of the sidewall boundary layer.

FIGURE 4. Surface oil-flow visualization.

The oil-flow results were compared with extrapolations of the flow angle profiles measured with the three-hole yawmeter. The maximum difference between the two methods was 3.5°, with the angle from the extrapolation being low in the early stages of crossflow development and high downstream of the bend. The oil-flow method is regarded as more accurate: the discrepancy with the three-hole yawmeter results is small enough to imply good accuracy of the latter in the main part of the flow.

The variation of the local skin friction coefficient, $c_f \equiv \tau_w / \frac{1}{2}\rho Q_e^2$, where $Q_e/U_{ref} = (1 - c_p)^{1/2}$, along the centreline of the tunnel is shown in Figure 5. As the flow entered the bend, c_f stopped its usual decrease with increasing Reynolds number and remained nearly constant well into the downstream section. Also included in the figure for comparison purposes are the values predicted from a 2DTBL correlation (Kays & Crawford 1993, p. 208), $c_f = 0.025 Re_\theta^{-0.25}$. The 2DTBL correlation tended to overpredict the skin friction in the upstream and bend regions, and did not predict increased skin friction in the downstream section.

The mean velocities U and W were measured both with the three-hole yawmeter and with the cross-wire hot-wire anemometer. The three-hole yawmeter measurements were preferred over the hot-wire mean-velocity measurements because the three-hole yawmeter was less susceptible to any calibration drift and less sensitive to mean-velocity gradient ($\partial U/\partial y$) effects. Additionally, the construction of the probes allowed the three-hole yawmeter to measure closer to the surface than the hot-wire anemometer.

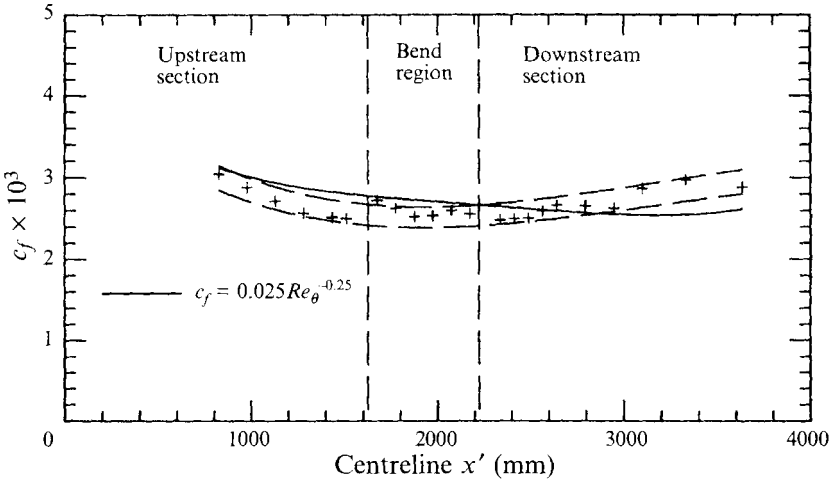

FIGURE 5. Axial variation of skin-friction coefficient. Dashed lines indicate 5% uncertainty bands.

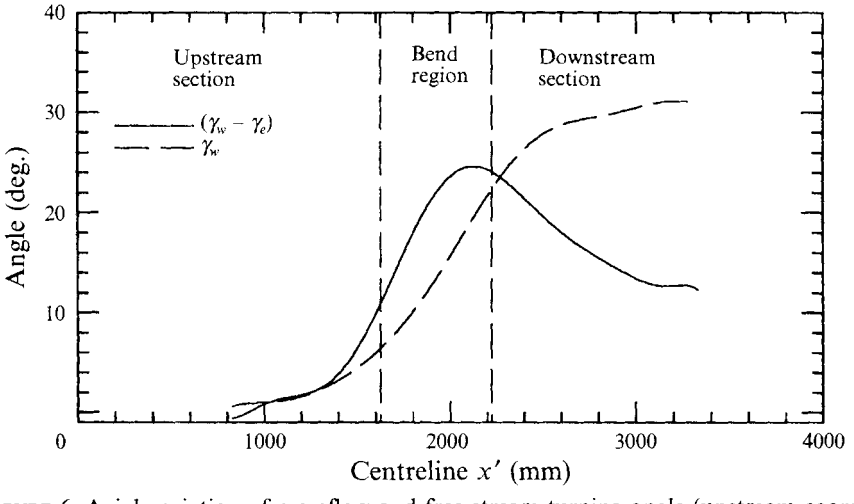

FIGURE 6. Axial variation of crossflow and free-stream turning angle (upstream coordinates).

The axial variation of the free-stream turning angle ($\gamma_e \equiv \tan^{-1} W_e/U_e$) relative to upstream coordinates and the surface crossflow relative to the free-stream direction ($\gamma_w - \gamma_e$) are shown in figure 6. The peak in surface crossflow occurred near the exit of the bend region. In the downstream section, the crossflow decreased gradually. The behaviour of the free-stream turning angle in the upstream and bend regions was similar to that of the crossflow angle. At the beginning of the downstream section, the rapid increase of the free-stream turning angle ceased and it began to approach 30° asymptotically.

Profiles of the normalized mean-velocity magnitude at locations along the tunnel centreline are shown in figure 7. The profiles gradually became fuller at least partly because the Reynolds number increased and a slight favourable pressure gradient developed downstream. It is not straightforward to attribute the reasons for the small changes in profile fullness due to potential three-dimensional effects. Table 1 summarizes several mean-flow boundary-layer parameters along the tunnel

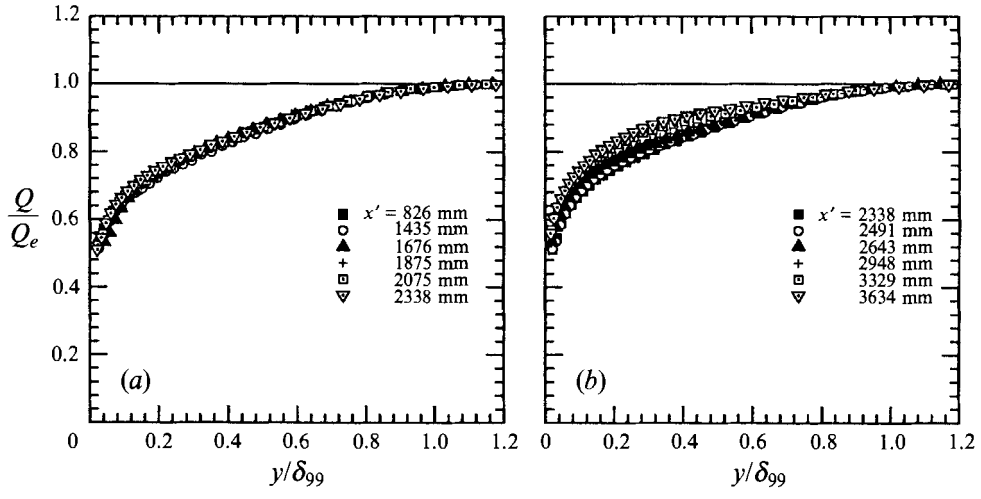

FIGURE 7. Mean-velocity magnitude: (*a*) crossflow development, (*b*) crossflow decay.

Station number	x' (mm)	δ_{99} (mm)	c_p -	c_f ($\times 10^6$)	Re_θ -	H -
0	826	20.92	0.0074	3039	4101	1.367
1	978	23.02	0.0052	2880	4584	1.373
2	1130	25.70	0.0037	2709	5249	1.377
3	1283	28.49	-0.0039	2567	6076	1.399
4	1435	31.22	0.0059	2514	6496	1.382
5	1511	32.15	0.0164	2499	6463	1.378
6	1676	32.22	0.0104	2720	6571	1.386
7	1775	30.91	0.0268	2622	6438	1.395
8	1875	32.65	0.0402	2521	6671	1.407
9	1975	33.72	0.0357	2534	6929	1.407
10	2075	35.25	0.0216	2598	7274	1.406
11	2174	36.95	0.0127	2555	7647	1.406
12	2338	39.15	0.0007	2481	8217	1.409
13	2415	39.97	-0.0129	2498	8351	1.399
14	2491	41.10	-0.0152	2502	8638	1.397
15	2567	42.23	-0.0228	2590	8761	1.379
16	2643	42.67	-0.0327	2663	8860	1.357
17	2796	44.58	-0.0442	2654	9047	1.344
18	2948	46.16	-0.0389	2628	9062	1.332
19	3100	47.81	-0.0535	2867	8985	1.309
20	3329	50.60	-0.0675	2969	8843	1.285
21	3634	53.22	-0.0620	2884	8588	1.280

TABLE 1. Boundary-layer integral parameters

centreline, including the boundary-layer thickness, static-pressure coefficient, skin-friction coefficient, Reynolds number based on momentum thickness, and shape factor. All are satisfactorily uneventful: this experiment was designed to investigate crossflow.

Using a non-dimensional resultant velocity and distance based on wall shear stress, $Q^+ \equiv Q/(\tau_w/\rho)^{1/2}$ and $y^+ \equiv y(\tau_w/\rho)^{1/2}/\nu$, the mean-velocity-magnitude profiles are

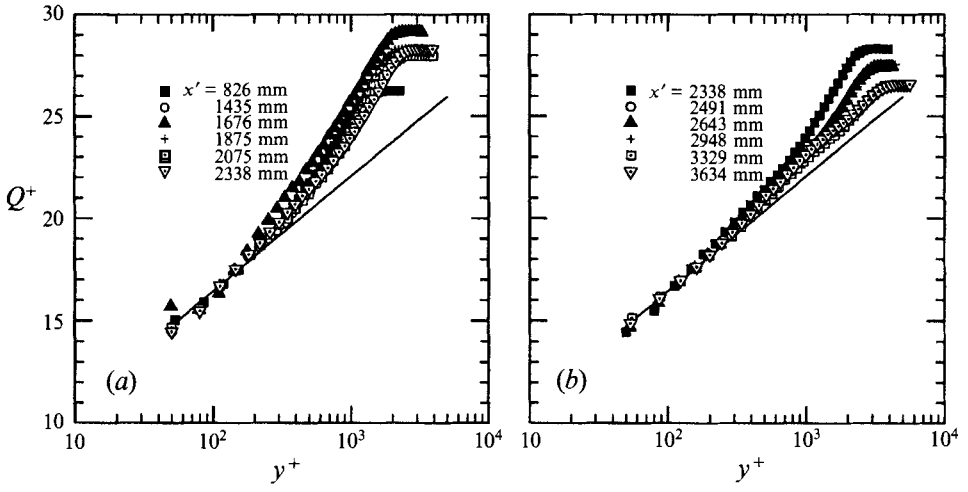

FIGURE 8. Mean-velocity profiles plotted using non-dimensional wall units: (*a*) crossflow development, (*b*) crossflow decay.

shown on log-linear axes in figure 8. A straight line representing a logarithmic law

$$Q^+ = 2.44 \ln y^+ + 5.2 \tag{7}$$

is also shown. The Flack & Johnston (1993) near-wall investigation showed that a similar logarithmic law agreed with their 3DTBL data. The profiles in the present work matched the logarithmic law of the wall until $y/\delta_{99} \approx 0.15$. The resultant velocity in the logarithmic region was close to the velocity component in the direction of the wall shear stress. In the wake region, however, there was considerable variation depending on the profile location. The overall trend was that the wake component grew from a moderate strength characteristic of 2DTBLs to a maximum in the bend before it decreased downstream. Typically, large increases in the velocity profile above that predicted by the logarithmic law are characteristic of 2DTBLs having adverse streamwise pressure gradients. Although there were not any significant adverse pressure gradients along the tunnel centreline, fluid migrating from the concave side of the bend towards the centreline had already undergone regions of adverse pressure gradient. Thus, the wake behaviour in this experiment can be explained qualitatively by the effects of pressure gradient and is not necessarily a three-dimensional effect as such.

Profiles of the crossflow angle relative to the direction of the free stream are shown in figure 9. The peak crossflow magnitude increased with the distance travelled in the test section until the end of the bend section where the maximum crossflow was approximately 25°. Downstream of the bend, the crossflow decayed slowly.

A traditional way to view the mean-velocity characteristics of a 3DTBL, due to Gruschwitz (1935), is to construct a 'triangular' plot of the normal and streamwise components of velocity relative to the free-stream velocity vector. For flows with small turning angles ($\sin\gamma_e \approx \gamma_e$, i.e. $\gamma_e < 15°$) and small velocity defects, the inviscid Squire–Winter–Hawthorne (SWH) relationship, Squire & Winter (1951) and Hawthorne (1951)

$$\frac{U_n}{Q_e} = 2\gamma_e\left(1 - \frac{U_s}{Q_e}\right) \tag{8}$$

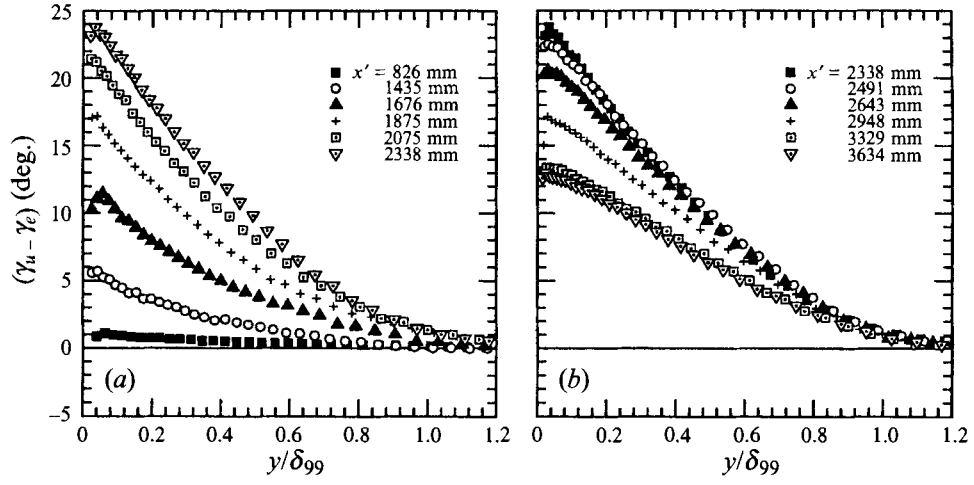

FIGURE 9. Crossflow angle relative to free stream: (*a*) crossflow development, (*b*) crossflow decay.

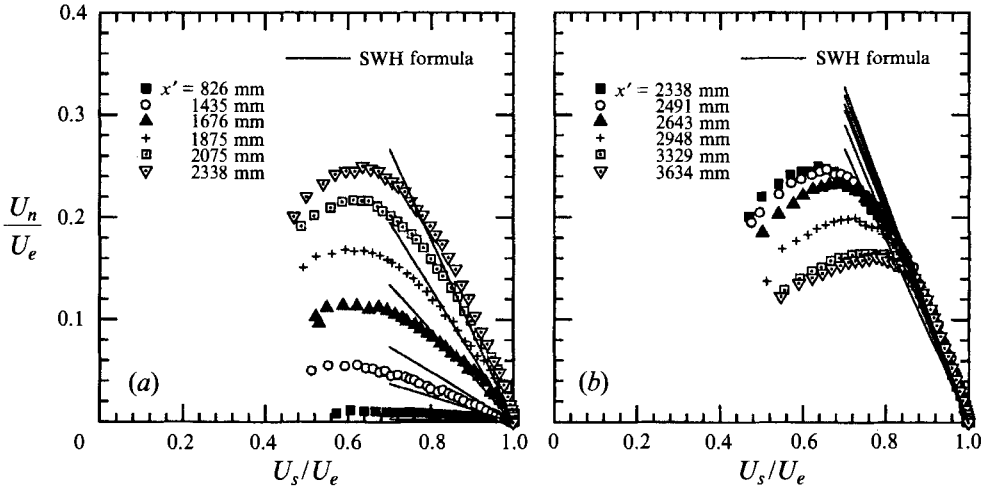

FIGURE 10. Triangular plot of velocity: (*a*) crossflow development, (*b*) crossflow decay.

can be used as a rough crossflow model with which to compare the present data. U_s and U_n are the streamwise and normal velocity components with respect to the free-stream velocity vector, whose magnitude is Q_e. The SWH relationship, shown above in the form used by Johnston (1960), states that the velocity in the outer layer should have a slope equal to twice the angle γ_e through which the free stream has turned. For this experiment, SWH fit the crossflow only in the outer half of the boundary layer ($y/\delta_{99} > 0.5$) as shown in figure 10. Exceptions to that agreement occurred in the bend where SWH underestimated the crossflow. The strong spanwise pressure gradient there may have been partly responsible. Other experimenters have usually found good agreement with SWH, implying that, in the outer layer, shear stresses are slow to reduce rapidly imposed crossflow. The distance from the surface at which the plots deviate from the SWH lines cannot be exactly identified with the outer edge of the region of significant cross-stream shear stress, but that region is certainly a thin and slowly growing internal layer.

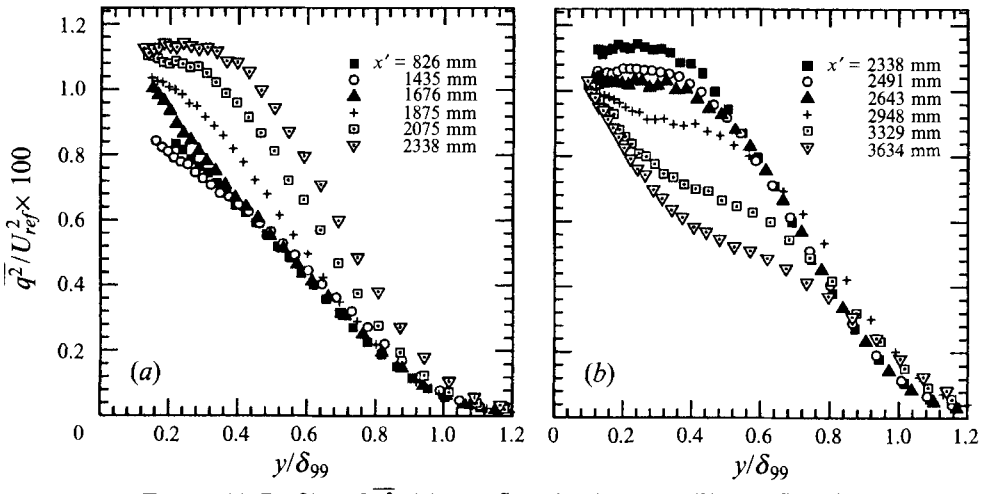

FIGURE 11. Profiles of $\overline{q^2}$: (*a*) crossflow development, (*b*) crossflow decay.

The $\overline{q^2}$ profiles shown in figure 11 were normalized by the external-flow velocity at the entrance of the test section, U_{ref}, to show absolute changes. Upstream of the bend, the outer-layer $\overline{q^2}$ profiles decreased in magnitude with axial distance, scaling with the square of the friction velocity. Then, as crossflow developed in the bend, $\overline{q^2}$ increased across the outer layer relative to upstream 2DTBL levels. The increase occurred mainly because the crossflow velocity gradient $\partial W/\partial y$ increased production in the outer layer. An apparent outer-layer peak developed at $y/\delta_{99} \approx 0.3$. Just downstream of the bend, crossflow decayed slowly and the increased levels persisted. Later, as crossflow decreased more rapidly, $\overline{q^2}$ began to decrease. The decrease began in the inner part, and then spread outward. In the outermost part of the boundary layer, $\overline{q^2}$ at a given y/δ_{99} was nearly constant. The overall behaviour was a rapid rise in mid-layer during crossflow development which then propagated outward like a solitary wave or 'bore' as crossflow decayed.

This kind of outward propagation has been found in various two-dimensional flows, notably boundary layers with short regions of surface curvature (in the x,y-plane). It suggests that turbulent transport is a combination of bulk convection by the larger eddies and diffusion by the smaller ones, rather than the pure gradient transport assumed in most turbulence models. The broad conclusion is that history effects were important as the outer layer remained relatively unaffected until changes near $y/\delta_{99} \approx 0.2$ had time to diffuse outward.

The Reynolds-stress data for the outer layer are shown in figures 12 and 13. Profiles of $\overline{u^2}$, $\overline{v^2}$, and $\overline{w^2}$ show increases with axial distance in all three normal stresses. Growth in $\overline{u^2}$ and $\overline{w^2}$ was due to increased production ($\overline{uv}\partial U/\partial y$ and $\overline{vw}\partial W/\partial y$) while the increase in $\overline{v^2}$ was due to pressure–strain redistribution. The $-\overline{uv}$ profiles behaved similarly to the $\overline{q^2}$ profiles. The increases in $-\overline{uv}$ resulted from elevated $\overline{v^2}$ values which contributed to production ($\overline{v^2}\partial U/\partial y$) as the crossflow developed. Downstream of the bend, $-\overline{uv}$ decayed. The $\overline{vw}$ stresses were smaller than the $-\overline{uv}$ stresses. Note that since the sense of z has been chosen to make W positive, $\partial W/\partial y$ and the (y,z)-plane shear stress $-\overline{vw}$ were negative except near the surface where W fell to zero. The $\overline{vw}$ stress, whose primary generation term is $\overline{v^2}\partial W/\partial y$, grew from nominally zero in the 2DTBL region to approximately 20% of $-\overline{uv}$ when the maximum surface

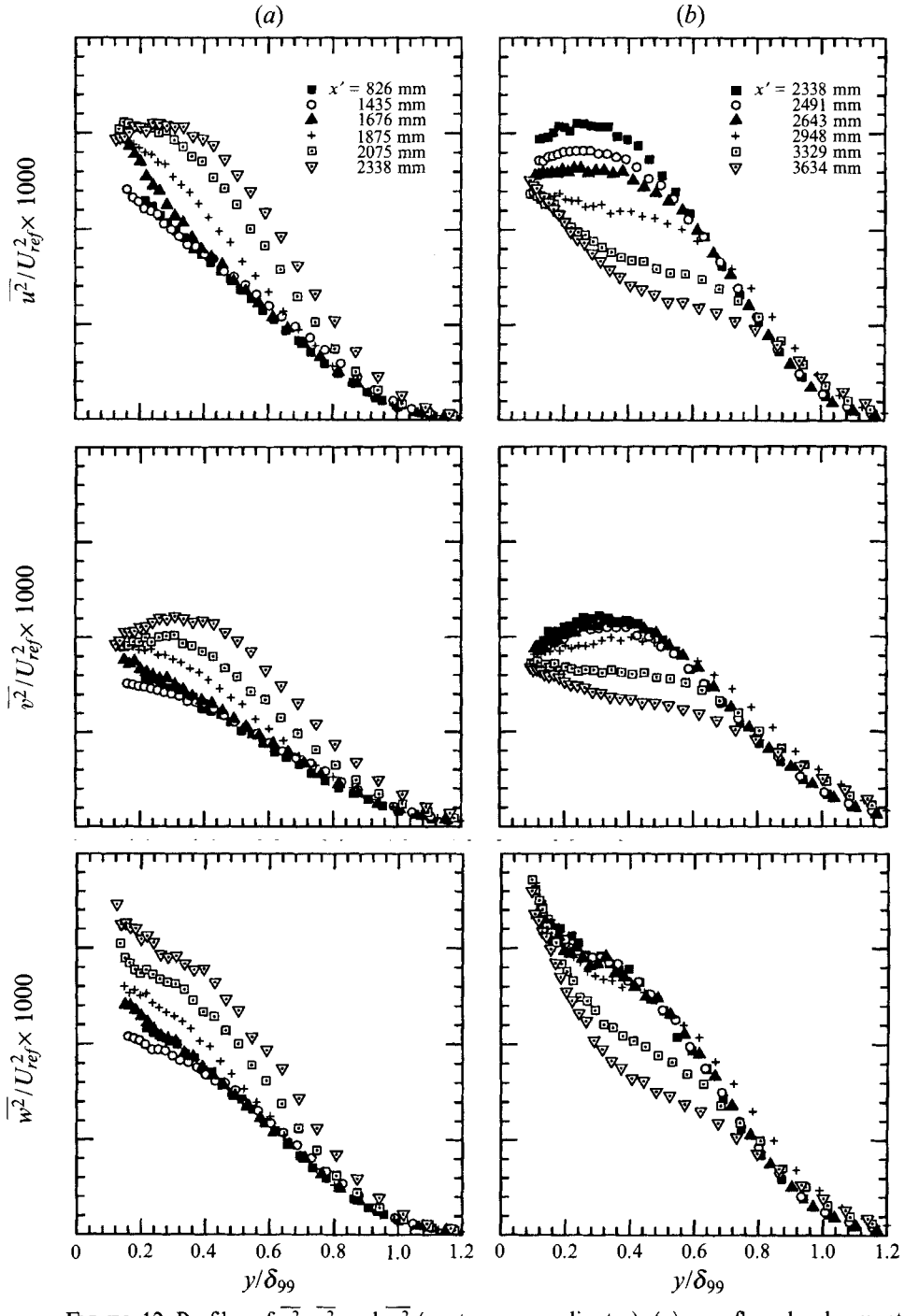

FIGURE 12. Profiles of $\overline{u^2}$, $\overline{v^2}$ and $\overline{w^2}$ (upstream coordinates): (*a*) crossflow development, (*b*) crossflow decay.

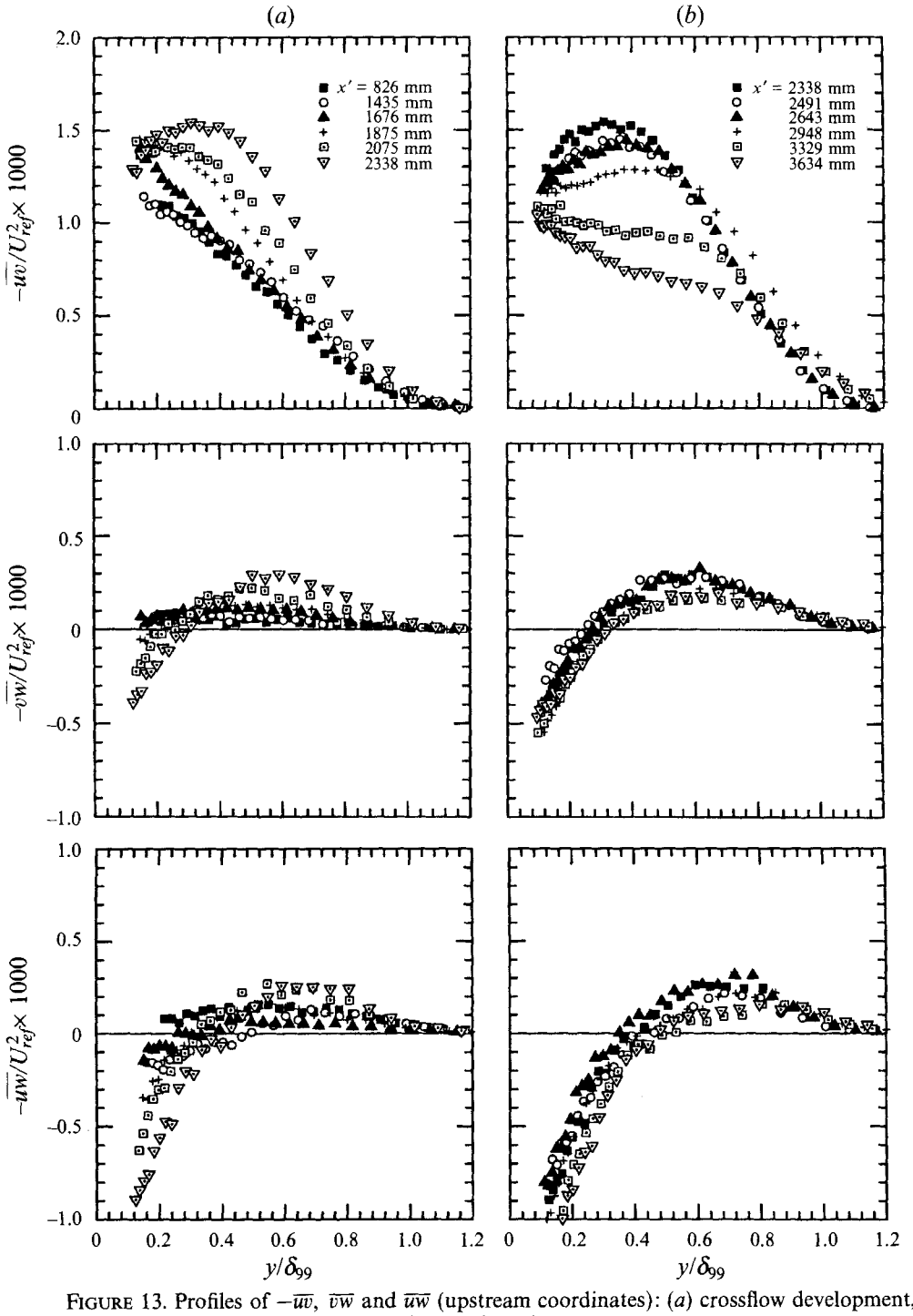

FIGURE 13. Profiles of $-\overline{uv}$, $\overline{vw}$ and $\overline{uw}$ (upstream coordinates): (*a*) crossflow development, (*b*) crossflow decay.

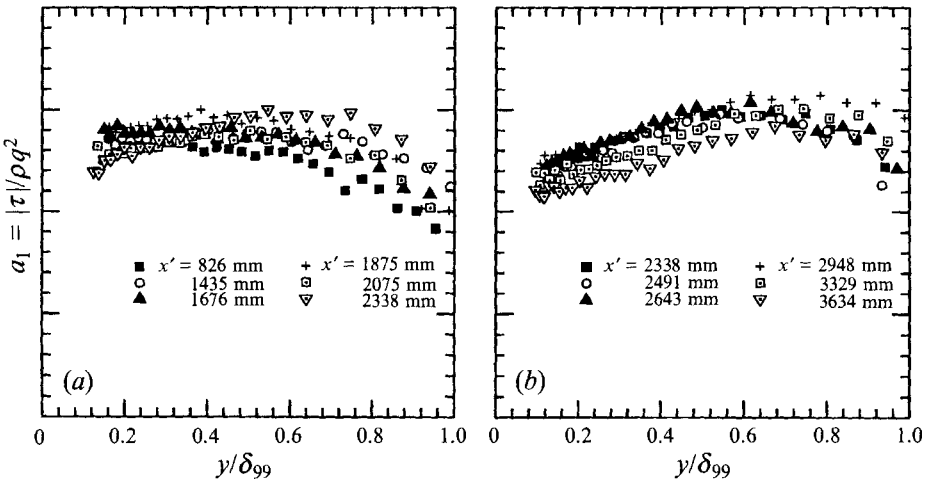

FIGURE 14. Profiles of the a_1 turbulence structure parameter: (*a*) crossflow development, (*b*) crossflow decay.

crossflow occurred. The $-\overline{uw}$ profiles show significant growth in the bend followed by a decrease in the downstream 3DTBL decay region. The 3DTBL approximation neglects gradients of $-\overline{uw}$, and indeed $-\overline{uw}$ was not important in the transport of either $-\overline{uv}$ or $\overline{vw}$.

In previous 3DTBL experiments, a_1 (stress/energy ratio) decreased relative to its 2DTBL value. Since most 3DTBL experiments show a decrease in a_1, one might conclude that crossflow is responsible for the decrease; however, the amount of the decrease varies greatly from experiment to experiment. This variation is probably due in part to the experiments having different streamwise pressure gradients as well as different degrees of crossflow.

Spalart & Watmuff (1993), using both experiments and direct numerical simulations, also saw a_1 decrease in two-dimensional boundary layers having adverse pressure gradients. Earlier, Bradshaw (1967) showed that an adverse pressure gradient in a 2DTBL increases *inactive* motions which can decrease a_1. Inactive motions do not affect $-\overline{uv}$ (because they do not affect v much). The a_1 parameter decreases because $\overline{u^2}$ and $\overline{w^2}$ increase. In an adverse pressure gradient where the turbulent shear stress decreases near the wall, inactive motion is expected to be a larger fraction of $\overline{q^2}$. Inactive motion may not be a complete explanation, but it certainly shows that the behaviour of a_1 can depend on pressure gradient as well as on crossflow.

In the present experiment, without any significant adverse streamwise pressure gradient along the centreline, the a_1 parameter displayed in figure 14 showed a moderate reduction to approximately 0.12 near $y/\delta_{99} \approx 0.2$ by the beginning of the downstream test section. In the outer half of the boundary layer, a_1 increased. At this station, crossflow was near its maximum. In the downstream section, as the crossflow decreased, a_1 decreased slightly further. The changes in a_1 reflect the differences in the behaviour of the resultant shear stress (dominated by $-\overline{uv}$) and of $\overline{q^2}$ and are thus linked to the behaviour of the outward-propagating bore mentioned above.

Figure 15 compares the angles, relative to the test section centreline, of the velocity vector, the shear-stress vector, and the velocity-gradient vector for two stations along the centreline of the test section. At x'=2075 mm in the bend region, the characteristic lagging of the shear-stress vector behind the velocity-gradient vector

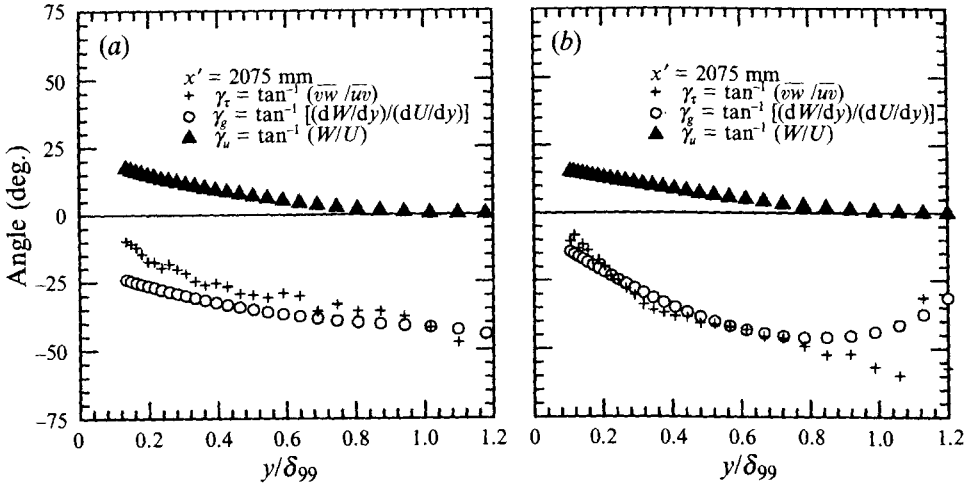

FIGURE 15. Shear-stress direction: (*a*) crossflow development, (*b*) crossflow decay.

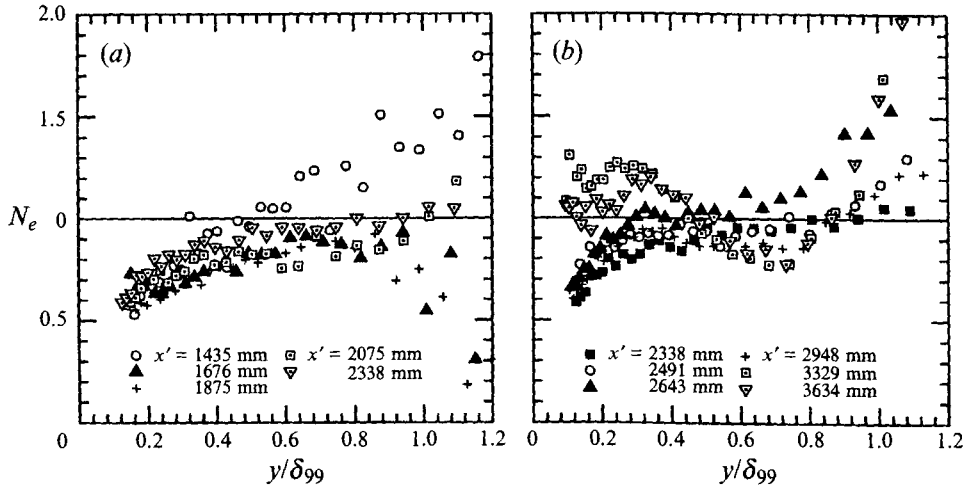

FIGURE 16. Profiles of the eddy-viscosity ratio (upstream coordinates): (*a*) crossflow development, (*b*) crossflow decay.

was clear. Further downstream at x'=2796 mm, the lag had decreased as the flow gradually relaxed back to a 2DTBL. The observed lagging of the shear-stress vector and the dependence of the lag on location indicate that, as in previous experiments on 3DTBLs, the Reynolds-stress behaviour would not be adequately predicted by isotropic eddy-viscosity models. Moreover, different parts of the boundary layer experienced varying amounts of lag suggesting that some type of $f(y/\delta)$ dependence would be needed even in anisotropic eddy-viscosity models.

The eddy-viscosity ratio profiles in figure 16 show that N_e decreased to as low as 0.6 in the crossflow development region and later recovered towards 1.0 as crossflow decayed. The reduction in N_e was intermediate between that of other experiments such as that of Anderson & Eaton (1989), for which N_e decreased to 0.2, and that of Elsenaar & Boelsma (1974), for which N_e decreased to 0.7. Anderson & Eaton (1989) theorized that the reduction was related to a non-dimensional free-stream turning

rate defined as the ratio of boundary-layer thickness to the radius of curvature of the free-stream streamline (δ/R). The N_c values in the present experiment agreed with the trend that flows with larger non-dimensional turning rates experience larger decreases, which is easy to understand from the transport equation for $\overline{vw}$: the more rapidly the crossflow builds up, the more $-\overline{vw}$ lags behind.

The acquisition of a complete set of triple-product measurements was important because relatively few 3DTBL experiments have included these data, which are necessary to evaluate the turbulent-diffusion terms in the Reynolds-stress transport equations. The main point is that if one measures the triple products and pressure diffusion is small, then the Reynolds-stress balances can be evaluated, with the dissipation and pressure–strain terms being found by difference. Figure 17 shows the $\overline{uv^2}$ and $\overline{v^2w}$ triple products important in the transport of $-\overline{uv}$ and $-\overline{vw}$. In the present experiment, $\overline{uv^2}$ increased its peak-to-peak variation and $\overline{v^2w}$ grew from nominally zero as the crossflow developed. The growth in the peak-to-peak variation was characteristic of all ten triple-products, implying increased turbulent transport of Reynolds stresses. Downstream of the bend, the peak-to-peak variations decreased in magnitude.

The action of the turbulence in transporting various quantities in the y-direction can be expressed as an effective vertical velocity *without* invoking any eddy-diffusivity concepts. Instead of considering the $\partial\overline{vq^2}/\partial y$ term in the turbulent kinetic energy transport equation, we can define the following vertical transport velocity for $\overline{q^2}$:

$$V_{q^2} = \overline{vq^2} / \overline{q^2}, \tag{9}$$

where $\overline{vq^2} = \overline{u^2v} + \overline{v^3} + \overline{vw^2}$. Note that this quantity nominally tends to 0/0 outside the boundary layer (as would an eddy diffusivity) so that measured values in the outer part of the boundary layer will be scattered. Figure 18 shows that $\overline{q^2}$ was generally transported away from the wall towards the free stream by the turbulent fluctuations in the upstream 2DTBL region, but it also shows that turbulent transport of $\overline{q^2}$ was altered in the presence of crossflow. At small y, the vertical transport reversed direction (negative V_{q^2}) while it was enhanced in the outer half of the boundary layer. This represents an important change in the physics of the boundary layer. The decrease in V_{q^2} was also observed in the 3DTBLs of Bradshaw & Pontikos (1985) and Anderson & Eaton (1989), and also in some 2DTBLs in an adverse pressure gradient, but this is apparently the first case where it can definitely be attributed to crossflow rather than pressure gradient. The efficient cause in either case is a peak in $\overline{q^2}$ moving away from the wall. The net downward transport implies that the inactive motion became stronger and/or that a peak in $\overline{q^2}$ at $y/\delta_{99} \approx 0.3$ started a gradient-diffusion-like transport. Vertical transport velocities were also calculated for the two important shear stresses: $V_{uv} = \overline{uv^2}/\overline{uv}$ and $V_{vw} = \overline{v^2w}/\overline{vw}$. The vertical transport of $\overline{uv}$ exhibits trends which were similar to those seen for V_{q^2}. However, the values were different by a factor of about 2, so that V_{q^2} and V_{uv} could not both be regarded as typical v-component velocities of the large eddies. This result can be explained by looking at the Reynolds-stress balances. Near the edge of the boundary layer, the production and dissipation terms in the turbulent kinetic energy balance approach zero much faster than the other terms. Therefore, the advection term equals the diffusion term so the entrainment velocity equals V_{q^2}. However, in the $-\overline{uv}$ balance, the pressure–strain term (not present in the turbulent kinetic energy transport equation) remains significant near the edge, so that V_{uv} does not equal V_{q^2}.

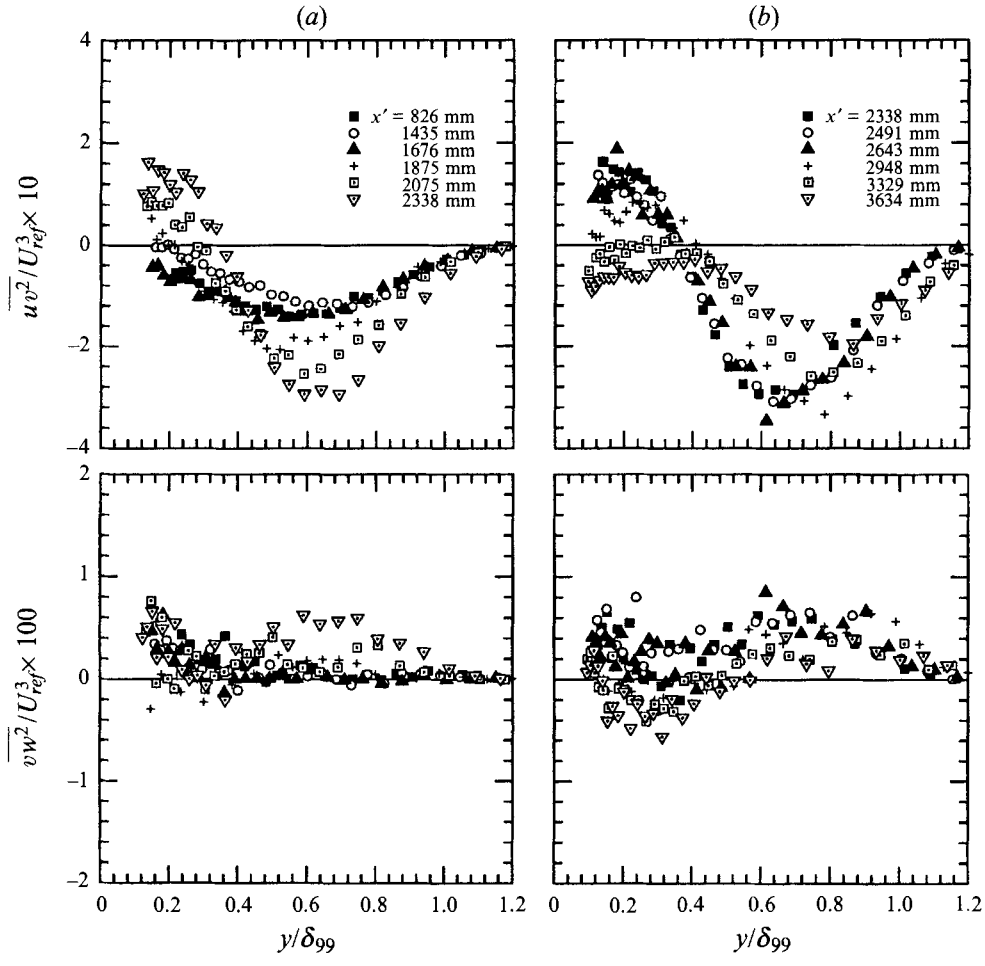

FIGURE 17. Profiles of $\overline{uv^2}$ and $\overline{v^2w}$ (upstream coordinates): (*a*) crossflow development, (*b*) crossflow decay.

Thus, the effective vertical velocity of turbulence is not universal: the transport of $\overline{vw}$ had a trend similar to those seen for $\overline{uv}$ but had a lower effective velocity.

Other statistical measures of the turbulence include the skewness and flatness (or kurtosis) of the velocity fluctuations. For the v-fluctuations

$$S_v = \overline{v^3}/(\overline{v^2})^{3/2} \quad \text{and} \quad F_v = \overline{v^4}/(\overline{v^2})^2. \tag{10}$$

Comparisons of the skewness and flatness at different axial locations are shown in figure 19. The outer-layer profiles collapsed well when the height was normalized by the boundary-layer thickness. The intermittency factor of the turbulence can be roughly estimated, using the flatness factor, as $\gamma = 3/F_v$.

The measurable terms in the Reynolds-stress transport equations were evaluated at seven locations along the tunnel centreline. Arbitrarily, a Cartesian coordinate system (x', y', z') aligned with the local tunnel centreline was used to study the transport. The Reynolds-stress transport equations are

$$U_l(-\overline{u_iu_j})_{,l} = \mathscr{P}_{ij} + \Phi_{ij} - \mathscr{D}_{ij} + \mathscr{J}_{ijk,k}, \tag{11}$$

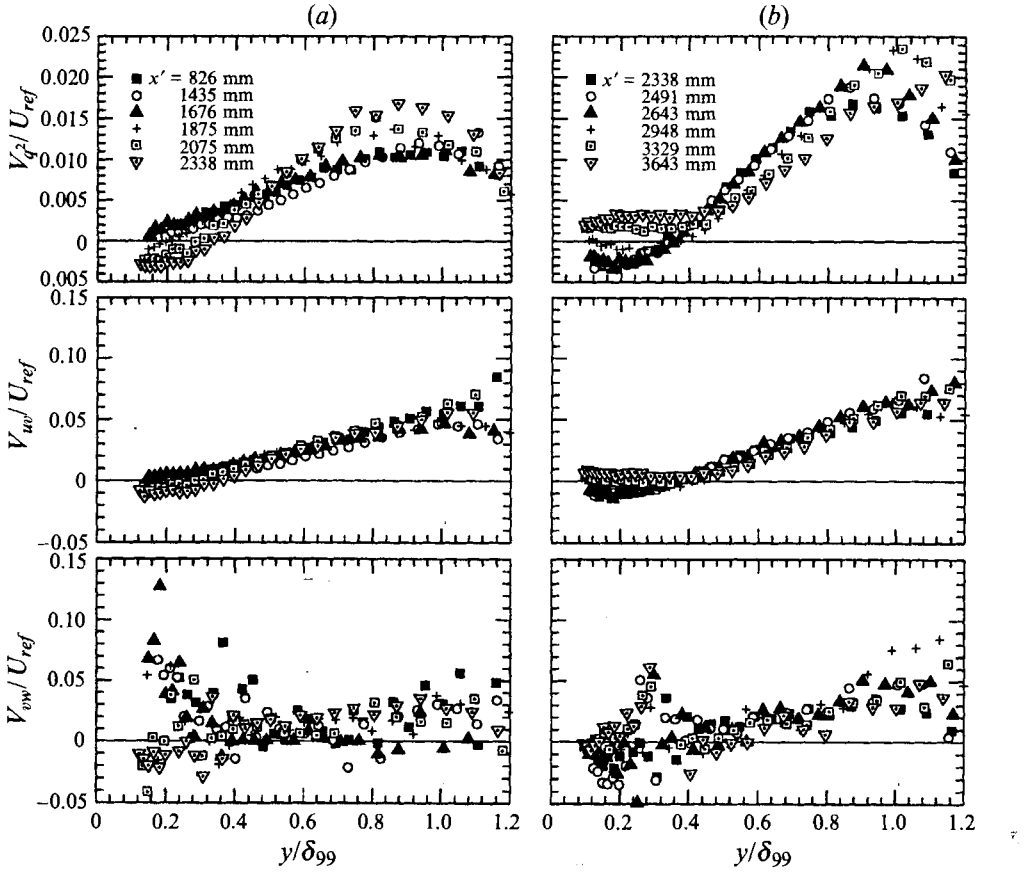

FIGURE 18. Vertical transport velocities (upstream coordinates): (*a*) crossflow development, (*b*) crossflow decay.

where the generation term $\mathscr{P}_{ij}$, the pressure–strain redistribution term Φ_{ij}, the viscous-destruction term $\mathscr{D}_{ij}$, and the flux of $-\overline{u_i u_j}$ in the x_k'-direction, $\mathscr{J}_{ijk}$, are defined by

$$\mathscr{P}_{ij} \equiv \overline{u_i u_k} U_{j,k} + \overline{u_j u_k} U_{i,k}, \tag{12}$$

$$\Phi_{ij} \equiv -\frac{1}{\rho}\overline{p'(u_{i,j} + u_{j,i})}, \tag{13}$$

$$\mathscr{D}_{ij} \equiv 2\nu \overline{u_{i,k} u_{j,k}}, \tag{14}$$

$$\mathscr{J}_{ijk} \equiv \frac{1}{\rho}(\overline{p'u_i}\delta_{jk} + \overline{p'u_j}\delta_{ik}) + \overline{u_i u_j u_k} + \nu(\overline{u_i u_j})_{,k}. \tag{15}$$

The turbulent kinetic energy transport equation,

$$U_l(\overline{q^2}/2)_{,l} = -\mathscr{P}_{ii} + \mathscr{D}_{ii} - \mathscr{J}_{iik,k}, \tag{16}$$

is slightly simpler because the pressure-strain term is trace-free, i.e. $\Phi_{ii}=0$. Derivatives of mean velocities, Reynolds-stresses, and triple products were calculated using central finite differences. Before calculating the derivatives, the data were smoothed in the vertical direction. Since the largest gradients were in the y'-direction, where the data points were closely spaced, and the measured quantities varied smoothly in the (x'-z')-plane, the uncertainties due to finite difference approximations were considered

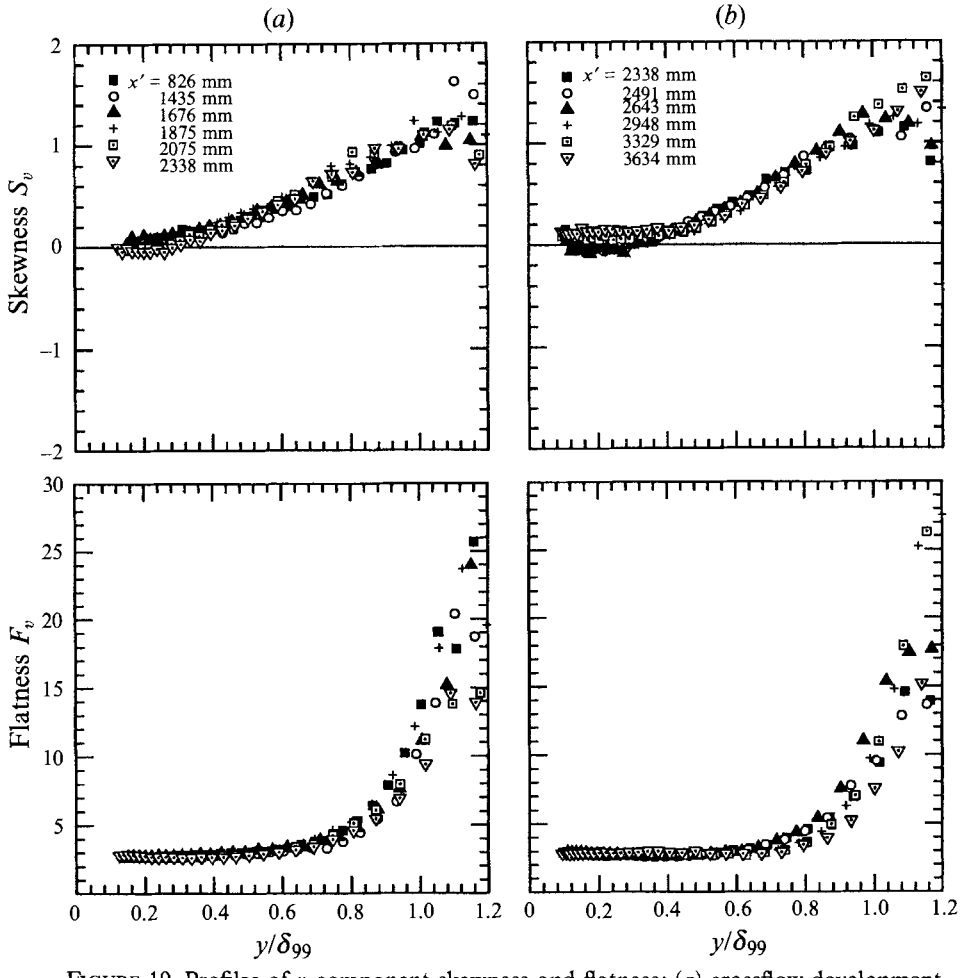

FIGURE 19. Profiles of v-component skewness and flatness: (*a*) crossflow development, (*b*) crossflow decay.

small (similar in magnitude to the uncertainties of the measured turbulence statistics). Terms were non-dimensionalized by multiplying by δ_{99}/U_{ref}^3 to show relative changes in magnitude.

The measured data allow most of the terms to be evaluated and the other major terms to be deduced by difference. Viscous transport terms were negligible everywhere. Some terms were not measured because accurate measurements would have been very difficult (dissipation) or because no instrumentation existed to make the measurements (pressure fluctuations). The dissipation was indirectly evaluated as the sum of all the other terms in the turbulent kinetic energy transport equation. This involved neglecting the contribution of pressure fluctuations to the diffusion term $\mathscr{J}_{ijk}$. Alternatively, the pressure diffusion could have been modelled using a model developed by Lumley (1978), $-(1/\rho)\overline{p'u_k} = \frac{1}{5}\overline{u_k q^2}$, to estimate the pressure–diffusion term. In most 2DTBLs, the role of turbulent transport via the triple products is small relative to production terms, except near the edge where the production term approaches zero faster than the diffusion term. The triple-product diffusion term usually balances the advection term near the edge, so the pressure transport is indeed

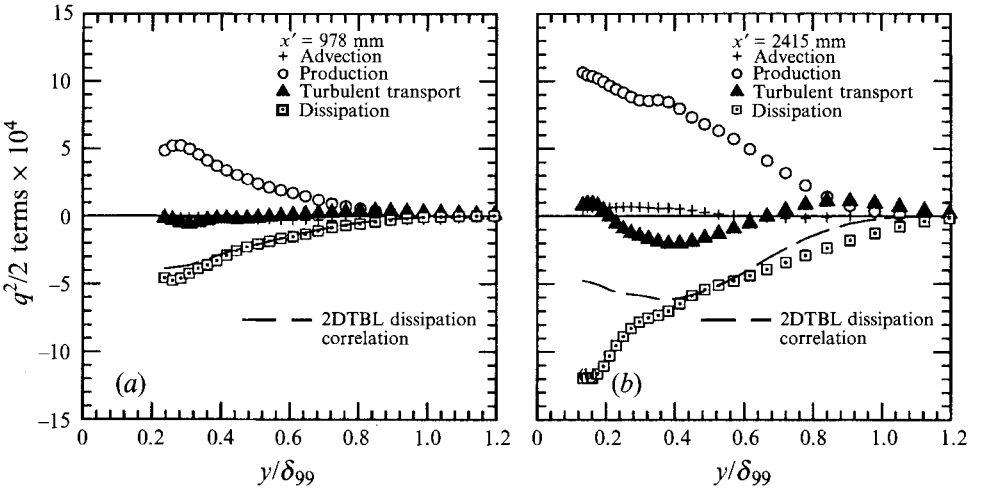

FIGURE 20. Turbulent kinetic energy transport: (*a*) 2DTBL region, (*b*) 3DTBL region. (Terms non-dimensionalized by δ_{99}/U_{ref}^2).

negligibly small near the edge – and hopefully elsewhere. Thus, the pressure–diffusion term was neglected: any error appears in the dissipation term.

Figure 20 compares the turbulent kinetic energy budgets for 2DTBL and 3DTBL locations, stations 1 and 13 in figure 1 (see Schwarz & Bradshaw 1992 for transport-equation terms at other locations). In the 2DTBL region, in the inner half of the boundary layer, advection and turbulent transport were small, so the estimated dissipation was roughly equal to the production. The estimated dissipation should therefore be about as accurate as the Reynolds-stress measurements. Near the edge of the boundary layer, the estimated dissipation approached zero faster than the transport terms, as expected. The main effects of crossflow were increases in production, dissipation, and turbulent transport. The contribution of $-\overline{vw}\partial W/\partial y'$ to the production is always small compared to $-\overline{uv}\partial U/\partial y'$, either in fixed upstream axes or axes referenced to the local centreline.

Bradshaw & Pontikos (1985), Moin *et al.* (1990), and Littell & Eaton (1991) found that the dissipation rate of turbulent kinetic energy was affected by the three-dimensionality of the mean flow. The dissipation rates in their 3DTBLs were consistently larger than those predicted by an empirical formula for the outer layer, $\epsilon = (\tau/\rho)^{3/2}/0.1\delta$, which works well in 2DTBLs. The dissipation rate predicted using the 2DTBL correlation is indicated by dashed lines in the figure. In the 3DTBL region, the 'measured' dissipation rate exceeded that predicted by the 2DTBL correlation. This disagreement probably occurred because the local equilibrium assumption of the correlation neglected the increased role of turbulent diffusion present in the 3DTBL region. The lumping of the pressure-diffusion term into the dissipation term would not have caused such large differences.

Figure 21 compares the terms in the $-\overline{uv}$ and $-\overline{vw}$ budgets for both 2DTBL and 3DTBL regions.

In the 2DTBL region, the $-\overline{uv}$ production and pressure–strain terms were larger in magnitude than the corresponding advection and turbulent transport terms again as in previous 2DTBL experiments. In the 3DTBL region, the advection and turbulent transport terms became larger, due primarily to $\overline{v^2}\partial U/\partial y'$ and to a lesser extent to

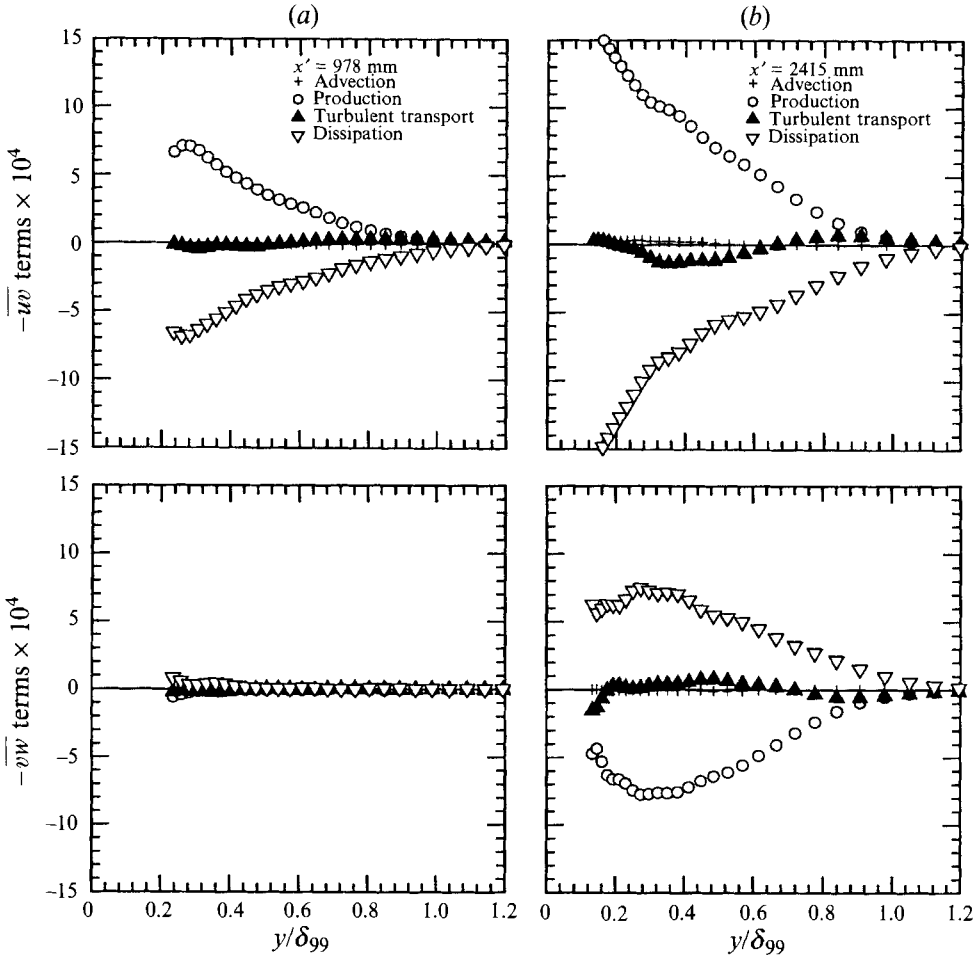

FIGURE 21. $-\overline{uv}$ and $-\overline{vw}$ transport (local coordinates): (*a*) 2DTBL region, (*b*) 3DTBL region. (Terms non-dimensionalized by δ_{99}/U_{ref}^2).

$\overline{vw}\partial U/\partial z'$ (negligible to the boundary-layer approximation). Increased production from $\overline{v^2}\partial U/\partial y'$ was mainly due to increases in $\overline{v^2}$ via pressure–strain redistribution: $\partial U/\partial y'$ changes little. The shear stresses near the edge of the boundary layer could not be characterized as being in a state of pure transport, like turbulent kinetic energy, because the pressure–strain term was still of the same order of magnitude as the advection and diffusion terms.

The terms in the $-\overline{vw}$ budget were negligible for x'=978 mm. However, the mean-flow velocity gradient $\partial W/\partial y'$ in the 3DTBL region, x'=2415 mm, promoted negative production of $-\overline{vw}$ (positive production of $\overline{vw}$), due to the right-handed turning of the flow which resulted in positive W values and negative $\partial W/\partial y'$ values. Turbulent transport and advection of $-\overline{vw}$ had much smaller magnitudes than the production term, so the pressure–strain redistribution term was approximately equal and opposite to production except near the edge.

4. General discussion and conclusions

The present experiment was designed to produce strong crossflow without the strong streamwise pressure gradients that have complicated the interpretation of previous experiments. The bend applies crossflow in a fairly short streamwise distance, so the flow approximates the response of an initially 2DTBL to a step increase in longitudinal mean vorticity $\partial W/\partial y$. The Reynolds shear stress $\overline{vw}$ is slow to affect $\partial W/\partial y$, except near the surface, so that changes to the large-eddy structure take place in a nearly frozen crossflow. The bend angle is sufficiently small that the sidewall boundary layers do not contaminate the floor boundary layer in the test region. This was the cleanest experiment we could devise to show up the effect of crossflow on turbulence structure in the outer layer with as few extraneous effects as possible. The complete details of the experiment are contained in Schwarz & Bradshaw (1992) and the data set is available from the authors on floppy disk.

These measurements of the turbulence structure in the outer layer of a 3DTBL are qualitatively consistent with the findings in previous experiments, as noted earlier. In some previous cases the Reynolds stresses have actually decreased following the start of crossflow, but this depends on the details of the flow and, as our results show, is not an essential feature. It is more meaningful to consider dimensionless parameters such as a_1 (less efficient production of turbulent shear stress) and N_e (anisotropy of eddy viscosity) and behaviour such as shear-stress vector lag and changes in triple-product profile shape. Also, one should keep in mind that the structural changes in the outer layer need not necessarily be the same as in the inner layer, and that low-Reynolds-number effects on the outer layer may interact with three-dimensional effects (this last point applies particularly to simulations).

As well as giving information about structure, the present experiment provides new data for developing and testing turbulence models for 3DTBLs. It is clear that the eddy-viscosity concept cannot completely account for the observed Reynolds-stress behaviour in a three-dimensional flow, but maybe stress-transport models can provide some hope for successful predictions. The measurements were detailed enough for all terms in the six Reynolds-stress transport equations to be evaluated, either directly or by difference.

Using data from the present experiment, we have also compared several current models for the triple products and the pressure–strain terms (see Schwarz & Bradshaw 1994 for details). The triple-product transport models generally predicted the triple-product profile shapes, but erratically under predicted the magnitudes of the peak-to-peak variations. In contrast, most of the pressure–strain models performed well despite large differences in model complexity. Since the largest modelled transport-equation terms in the outer layer of a turbulent boundary layer are the pressure–strain and dissipation terms, the large errors in the triple-product models would not have much impact on Reynolds-stress predictions. Thus, the good performance of the pressure–strain models suggests that the model equation for dissipation is the main source of inaccuracy in complete prediction methods for 3DTBLs.

The next stage of investigating 3DTBL structure will be spatial correlation measurements. So far, the only correlation measurements in a three-dimensional flow were those made by Littell & Eaton (1991) and the only three-dimensional direct numerical simulation to include correlations was that of Sendstad & Moin (1991), where the information was restricted to the viscous wall region. Spatial correlations and/or conditional sampling measurements are needed to determine the structural causes of changes in one-point statistics.

In the long term, direct numerical simulation offers the best way to obtain quantities such as dissipation and pressure-fluctuation statistics, which we have had to estimate by difference. Direct numerical simulation is also giving useful information for the near-wall region, which otherwise requires measurements either in a very thick flow or with micro-instrumentation. However, direct numerical simulation is currently limited not only to simple flows, but also to Reynolds numbers which are so low that significant viscous effects occur in the outer layer. Therefore computer simulations will not replace wind-tunnel experiments for some time. Probably the most urgent need is for high-Reynolds-number experiments on more complex turbulent flows.

The authors gratefully acknowledge the support of the Boeing Company under contract number TO-582834-0757N, and helpful discussions with Dr S. F. Birch and Dr G. C. Paynter. W.R.S. is also grateful for support from the Scholarship Foundation of the Society of Experimental Test Pilots, and the encouragement of Mr Max Stanley. We would like to thank Dr S. V. Veeravalli for his help in the early stages of the experiment, and our colleagues Professors J. K. Eaton and J. P. Johnston for many fruitful discussions. The referees are also thanked for their helpful comments.

REFERENCES

ANDERSON, S. D. & EATON, J. K. 1987 An experimental investigation of pressure driven three-dimensional boundary layers. *Stanford University Thermosciences Div. Rep.* MD-49.

ANDERSON, S. D. & EATON, J. K. 1989 Reynolds stress development in pressure-driven three-dimensional turbulent boundary layers. *J. Fluid Mech.* **202**, 263–294.

BEARMAN, P. W. 1971 Corrections for the effect of ambient temperature drift on hot-wire measurements in incompressible flow. *DISA Rep.* **11**, May 1971, pp. 25–30.

BERG, B. VAN DEN 1990 Turbulence modelling: survey of activities in Belgium and the Netherlands, an appraisal of the status and a view on the prospects. *NLR Tech. Publication* 90184 L.

BISSONNETTTE, L. R. & MELLOR, G. L. 1974 Experiments on the behaviour of an axisymmetric turbulent boundary layer with a sudden circumferential strain. *J. Fluid Mech.* **63**, 369–413.

BRADSHAW, P. 1967 The turbulence structure of equilibrium boundary layers. *J. Fluid Mech.* **29**, 625–645.

BRADSHAW, P. 1990 Progress in turbulence research. *AIAA* 90-1480, presented at AIAA 21st Fluid Dynamics Meeting, Seattle, Washington.

BRADSHAW, P. & PONTIKOS, N. S. 1985 Measurements in the turbulent boundary layer on an 'infinite' swept wing. *J. Fluid Mech.* **159**, 105–130.

BRADSHAW, P. & TERRREL, M. G. 1969 The response of a turbulent boundary layer on an 'infinite' swept wing to the sudden removal of pressure gradient. *NPL Aero Rep.* 1305.

BRYER, D. W. & PANKHURST, R. C. 1971 *Pressure-Probe Methods for Determining Wind Speed and Flow Direction.* London: HMSO.

COLEMAN, G. N., FERZIGER, J. H. & SPALART, P. R. 1990 A numerical study of the turbulent Ekman layer. *J. Fluid Mech.* **213**, 313–348.

DECHOW, R. & FELSCH, K. O. 1977 Measurements of the mean velocity and of the Reynolds stress tensor in a three-dimensional turbulent boundary layer induced by a cylinder standing on a flat wall. In *Proc. of Symp. on Turbulent Shear Flows*, Vol. 1, April 18-20, 1977, *University Park, Pennsylvania.*

DEGANI, A. T., SMITH, F. T. & WALKER, J. D. A. 1992 The three-dimensional turbulent boundary layer near a plane of symmetry. *J. Fluid Mech.* **234**, 329–360.

DEGRANDE, G. & HIRSCH, C. 1978 Three-dimensional incompressible turbulent boundary layers. *Free Univ. of Brussels Rep.* VUB-STR-8.

DRIVER, D. M. & HEBBAR, S. K. 1987 Experimental study of a three-dimensional, shear-driven, turbulent boundary layer. *AIAA J.* **25**, 35–42.

DRIVER, D. M. & JOHNSTON, J. P. 1990 Experimental study of a three-dimensional shear-driven turbulent boundary layer with streamwise adverse pressure gradient. *NASA Tech. Mem.* 102211.

EAST, L. F. & SAWYER, W. G. 1979 Measurements of the turbulence ahead of a 45° swept step using a double split-film probe. *RAE Tech. Rep.* 79136.

EATON, J. K. 1991 Turbulence structure and heat transfer in three-dimensional boundary layers. *9th Symp. on Energy Engineering Sciences, Argonne National Laboratories.*

ELSENAAR, A. & BOELSMA, S. H. 1974 Measurements of the Reynolds stress tensor in a three-dimensional turbulent boundary layer under infinite swept wing conditions. *NLR TR*74095 U.

FANNELØP, T. K. & KROGSTAD, P. A. 1975 Three-dimensional turbulent boundary layers in external flows: a report on Euromech 60. *J. Fluid Mech.* **71**, 815–826.

FERNHOLZ, H. H. & VAGT, J. D. 1981 Turbulence measurements in an adverse pressure gradient three-dimensional turbulent boundary layer along a circular cylinder. *J. Fluid Mech.* **111**, 233–269.

FLACK, K. A. & JOHNSTON, J. P. 1993 Near-wall investigation of three-dimensional turbulent boundary layers. *Stanford University Thermosciences Div. Rep.* MD-63.

GRUSCHWITZ, E. 1935 Turbulente Reibungsschicten mit Sekundärströmungen. *Ing.-Arch.* **6**, 355–365.

HAWTHORNE, W. R. 1951 Secondary circulation in fluid flow. *Proc. R. Soc. Lond.* A **206**, 374–387.

JOHNSTON, J. P. 1960 On the three-dimensional turbulent boundary layer generated by secondary flow. *Trans. ASME* D:, *J. Basic Engng* **82**, 233–248.

JOHNSTON, J. P. 1970 Measurements in a three-dimensional turbulent boundary layer induced by a swept, forward-facing step. *J. Fluid Mech.* **42**, 823–844.

JOHNSTON, J. P. 1976 Experimental studies in three-dimensional turbulent boundary layers. *Stanford University Thermosciences Div. Rep.* MD-34.

KAYS, W. M. & CRAWFORD, M. E. 1993 *Convective Heat and Mass Transfer*, 3rd Edn. McGraw-Hill.

KLEBANOFF, P. S. 1954 Characteristics of turbulence in a boundary layer with zero pressure gradient. *NACA TN* 3178.

LAKSHMINARAYANA, B. 1986 Turbulence modelling for complex shear flows. *AIAA J.* **24**, 1900– 1917.

LAUNDER, B. E. 1988 Turbulence modelling of three-dimensional shear flows. *AGARD-CP*-438.

LITTELL, H. S. & EATON, J. K. 1991 An experimental investigation of the three-dimensional boundary layer on a rotating disk. *Stanford University Thermosciences Div. Rep.* MD-60.

LOHMANN, R. P. 1976 The response of a developed turbulent boundary layer to local transverse surface motion. *Trans. ASME* I: *J. Fluids Engng* **98**, 355–363.

LUMLEY, J. L. 1978 Computational modeling of turbulent flows. *Adv. Appl. Mech.* **18**, 123–176.

MOIN, P., SHIH, T. H., DRIVER, D. & MANSOUR, N. M. 1990 Direct numerical simulation of a three-dimensional turbulent boundary layer. *Phys. Fluids* A **2**, 1846–1853.

MÜLLER, U. R. 1982 Measurement of the Reynolds stresses and the mean-flow field in a three-dimensional pressure-driven boundary layer. *J. Fluid Mech.* **119**, 121–153.

MURLIS, J., TSAI, H. M. & BRADSHAW, P. 1982 The structure of turbulent boundary layers at low Reynolds numbers. *J. Fluid Mech.* **122**, 13–56.

ÖLÇMEN, S. & SIMPSON, R. L. 1992 Perspective: on the near-wall similarity of three-dimensional turbulent boundary layers. *Trans. ASME* I: *J. Fluids Engng*, **114**, 487–495.

PATEL, V. C. 1965 Calibration of the Preston tube and limitations on its use in pressure gradients. *J. Fluid Mech.* **23**, 185–208.

PIERCE, F. J. & DUERSON, S. H. 1975 Reynolds stress tensors in an end-wall three-dimensional channel boundary layer. *Trans. ASME* I, *J. Fluids Engng* **96**, 61–67.

PIERCE, F. J. & EZEKEWE, C. I. 1976 Measured $\overline{uw}$ stress gradients in a three-dimensional turbulent boundary layer. *Trans. ASME* I: *J. Fluids Engng* **98**, 6768–770.

PIERCE, F. J., MCALLISTER, J. E. & TENNANT, M. H. 1983 Near-wall similarity in a pressure-driven three-dimensional turbulent boundary layer. *Trans. ASME* I: *J. Fluids Engng* **105**, 257–262.

PURTELL, L. P. 1992 Turbulence in complex flows: a selected review. *AIAA* 92-0435, presented at 30th Aerospace Sciences Meeting, January 1992, Reno, Nevada.

SCHWARZ, W. R. & BRADSHAW, P. 1992 Three-dimensional turbulent boundary layer in a 30 degree bend: experiment and modelling. *Stanford University Thermosciences Div. Rep.* MD-61.

SCHWARZ, W. R. & BRADSHAW, P. 1994 Term-by-term tests of stress-transport models in a three-dimensional boundary layer. *Phys. Fluids* **6**, 986–998.

SENDSTAD, O. & MOIN, P. 1991 On the mechanics of 3-D turbulent boundary layers. in *Proc. 8th Turbulent Shear Flows Symp., Sept. 9-11, Munich, Germany.*

SPALART, P. R. 1989 Theoretical and numerical study of a three-dimensional turbulent boundary layer. *J. Fluid Mech.* **205**, 319–340.

SPALART, P. R. & WATMUFF, J. H. 1993 Experimental and numerical study of a turbulent boundary layer with pressure gradient. *J. Fluid Mech.* **249**, 337–372.

SQUIRE, H. B. & WINTER, K. G. 1951 The secondary flow in a cascade of airfoils in a nonuniform stream. *J. Aero. Sci.* **18**, 271–277.

YOUNG, A. D. & MAAS, J. N. 1936 The behavior of a Pitot tube in a transverse total-pressure gradient. *Aero. Res. Coun. R & M* 1770.